

# Diffusive motion of $C_{60}$ on a graphene sheet

M. Neek-Amal<sup>1</sup>\*, N. Abedpour<sup>2</sup>, S. N. Rasuli<sup>3</sup>, A. Naji<sup>3</sup> and M. R. Ejtehadi<sup>2</sup>

<sup>1</sup> Department of Physics, Shahid Rajaei University, Lavizan, Tehran 16788, Iran

<sup>2</sup> Department of Physics, Sharif University of Technology, Tehran 11155-9161, Iran

<sup>3</sup>School of Physics, Institute for Research in Fundamental Sciences, Tehran 19395-5531, Iran

November 1, 2018

## Abstract

The motion of a  $C_{60}$  molecule over a graphene sheet at finite temperature is investigated both theoretically and computationally. We show that a graphene sheet generates a van der Waals laterally periodic potential, which directly influences the motion of external objects in its proximity. The translational motion of a  $C_{60}$  molecule near a graphene sheet is found to be diffusive in the lateral directions. While, in the perpendicular direction, the motion may be described as diffusion in an effective harmonic potential which is determined from the distribution function of the position of the  $C_{60}$  molecule. We also examine the rotational diffusion of  $C_{60}$  and show that its motion over the graphene sheet is not a rolling motion.

---

\*Corresponding author: mehdi.neekamal@gmail.com

# 1 Introduction

Various properties of graphene as a new two dimensional material have been studied both experimentally and theoretically [1, 2]. A recent experimental research based on TEM visualization studies the images and dynamics of light atoms deposited on a single-layer graphene sheet [3]. On the other hand diffusion process and crystallization of atoms and light molecules on various surfaces have also been subject of research for many years due to both their theoretical importance as well as their technological applications. The theoretical studies of the motion of molecular scale objects on the various surface is also applicable to the motion of nanoscale object's over nanoelectromechanical surfaces, i.e., graphene. These studies play an important role in designing graphene based nanosensors. Diffusive motion of inclusions (*e.g.* macromolecules) over a rough membrane is another related subject, which has received a lot of attention in recent years [4, 5, 6]. Solidification of  $C_{60}$  molecules over various substrates particularly graphene is another subject of interest. The van der Waals epitaxy of a solid  $C_{60}$  over graphene sheet has been done in recent experiments [7]. Also various dynamical properties of the spinning motion of  $C_{60}$  on the Au(1 1 1) surface have been studied by Teobaldi *et al.* by means of molecular dynamics (MD) simulations [8].

The choice of van der Waals parameters of  $C_{60}$ -graphene interaction is an important issue for performing any molecular dynamics simulations. The  $C_{60}$ -carbon nanotubes interaction can be obtained both experimentally and theoretically [9]. Several van der Waals parameters for physical adsorption of  $C_{60}$  on graphite and other substrates were formulated using a continuum rigid body model for  $C_{60}$  and a continuum dielectric media for graphite by Girad *et al* [10]. The charge transfer from graphene to the  $C_{60}$  molecule is an open question which may be tackled using modern density functional theories. For alkali metals on the graphite there have been some calculations in order to estimate transferred charges [11].

Two main approaches for investigating the diffusive motion of an external inclusion on the membranes surface can be introduced. The first one is based on the continuum description for the membrane structure and introduces an effective Hamiltonian which can be used to study curvature-coupled diffusion [5, 4, 6]. The elastic aspects of the membrane thus play a key role in this approach. The second approach is an atomistic one which considers the details of the membrane and inclusion structures as well as atomic interactions on different levels of coarse graining [12, 13]. The main goal in these studies is to characterize the inclusion's motion.

The diffusive motion of particles may be modeled generally via a Langevin equation. Lacasta *et al* have modeled general two dimensional solid surfaces using a two dimensional potential both with a deterministic periodic potential and a random one [14]. Different values for dissipation parameters generate different trajectories for a point-like particle over such potentials, which thus lead to different dynamical behaviors ranging from subdiffusive to superdiffusive motion [14].

In a previous study we showed that the alkali and transition metals distribute over graphene and bind to its surface via a Lennard-Jones potential and construct atomic nanoclusters [16]. For metallic nanoclusters, no diffusive motion was found in low temperature. It is also found that potassium atoms, in low temperature, construct a particular phase on the graphene sheet as well as on the graphite [11]. To our knowledge there have been only a few number of studies on the interaction between graphene and inclusions that address the pattern of inclusion motion [4, 5, 6].

In this paper we study the dynamics of a single molecule, specifically chosen as the  $C_{60}$  molecule, on a graphene surface. We show that a graphene sheet creates a periodic van der Waals potential in its surrounding space and that there are some simple criteria to determine when a molecule may diffuse through the potential wells generated by the graphene (as assisted by thermal fluctuations) or be likely to be trapped in the potential wells near the surface. We introduce a laterally-averaged

effective potential for the graphene sheet from the distribution function of  $C_{60}$  near the surface, and show that this potential may be approximated best by a harmonic potential in the direction normal to the sheet. We also introduce an effective friction coefficient for the diffusive motion of  $C_{60}$  over graphene. Finally, we show that the motion of  $C_{60}$  over graphene is not a rolling motion and also the variation of the perpendicular component of angular velocity of  $C_{60}$  is greater than its component parallel to the graphene sheet.

## 2 Methods

We employ classical Molecular Dynamics (MD) algorithm to simulate the  $C_{60}$ -graphene system. The graphene is modeled as a square-like sheet of area  $1883 \text{ nm}^2$  constructed of 72000 carbon atoms. The temperature was kept constant (300K) in our simulations by employing a Nosé-Hoover thermostat. For the covalent bounds between the nearest neighbor atoms of the graphene sheet (and for chemically bonded atoms in  $C_{60}$  molecule) we have used Brenner's potential [17]. For the interaction between each atom of graphene with each of  $C_{60}$ 's atoms, we have used the Lennard-Jones potential (LJ),

$$U_{LJ} = 4\varepsilon\{(\sigma/r)^{12} - (\sigma/r)^6\}$$

with a typical values  $\sigma = 3.4 \text{ \AA}$  and  $\varepsilon = 2.4 \text{ meV}$  [15]. A graphene sheet was initially positioned, on average, at  $z = 0$  plane, and the centers of the  $C_{60}$  molecule were placed above it at  $z = 7 \text{ \AA}$ . The temperature-dependent molecular dynamics simulations run for up to two nanoseconds.

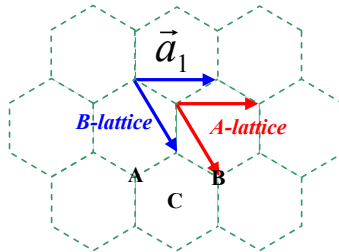


Figure 1: (Color online) Two common triangular sublattices of graphene sheet in the  $x - y$  plane.

## 3 Two dimensional potential of garphene sheet

First we study the periodic two dimensional LJ potential that a flat graphene sheet creates near its surface. Generally, graphene is not a flat sheet in finite temperature and exhibits small roughness; it may thus be locally approximated with a flat sheet [18]. The aforementioned quantity helps one to gain some insight into how graphene influences molecules such as  $C_{60}$  moving at its proximity.

A flat graphene sheet comprises two triangular Bravais sublattices (see Fig. 1), and the LJ potential due to this sheet [9] can be written as the sum of these two sublattice potentials

$$E_T(x, y, z) = V_{A-lattice} + V_{B-lattice}, \quad (1)$$

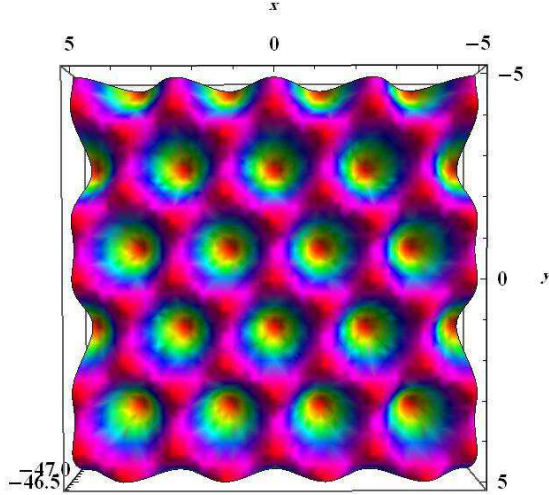


Figure 2: (Color online) Periodic two dimensional potential,  $\tilde{V}(x, y)$ , created by the graphene sheet. Here  $x$  and  $y$  refer to spatial position at the height  $z_0=3.5\text{\AA}$  above the graphene sheet. This figure shows the top view of the potential.

where  $(x, y, z)$  is the position for center of mass of the molecule, having  $N$  atoms, above the sheet. We may write the appropriate expression for  $V_{A-lattice}$  as

$$V_{A-lattice} = \sum_{m,n} \sum_{l=1}^N \sum_{k=1}^2 \frac{4(-1)^{k+1} \sigma^{12/k}}{((x + x_l - n - m/2)^2 + (y + y_l - \sqrt{3}m/2)^2 + (z + z_l)^2)^{6/k}} \quad (2)$$

and for  $V_{B-lattice}$  as

$$V_{B-lattice} = \sum_{m,n} \sum_{l=1}^N \sum_{k=1}^2 \frac{4(-1)^{k+1} \sigma^{12/k}}{((x + x_l + 1/2 - n - m/2)^2 + (y + y_l - \sqrt{3}m/2 - \sqrt{3}/6)^2 + (z + z_l)^2)^{6/k}} \quad (3)$$

Here  $m$  and  $n$  are integer numbers which count lattice points for each sublattice. The coordinate of the  $l^{th}$  atom  $(x_l, y_l, z_l)$  is measured from the molecule's center of mass. The sum over  $k$  also, is responsible for varying of fraction's power between 12 or 6, and switching its sign. Because of the short range behavior of the LJ potential, we observed that using the cut-offs of  $|m| \geq 10$  or  $|n| \geq 10$  leads to quite accurate results with negligible cut-off errors in the total potential/force. For simplicity in Eqs. (2) and (3) all lengths were re-scaled by  $a_1 = \sqrt{3}a_0$  where  $a_0 = 1.42 \text{\AA}$  and energies are in units of  $\varepsilon$ , with  $a_1$  being the length of primitive vector of sublattices (see Fig. 1).

### 3.1 Potential energy between a single carbon atom and graphene sheet

At a fixed height above the graphene sheet,  $z = z_0$ , the total potential in Eq. (1) reduces to a two-dimensional potential  $\tilde{V}(x, y)$ , which is periodic in  $x$  and  $y$ . Assume that we have fixed the height of a point like particle, such as a carbon atom, at a given value. Figure 2 shows this periodic two-dimensional potential for  $z_0=3.5 \text{\AA}$ . This potential provides some insights into the diffusive motion or trapping of a point-like particle close to the graphene sheet [3]. The required potential can be obtained from Eqs. (2) and (3) with  $N = 1$  and putting  $x_l, y_l$  and  $z_l$  equal to zero. Figure 3 shows

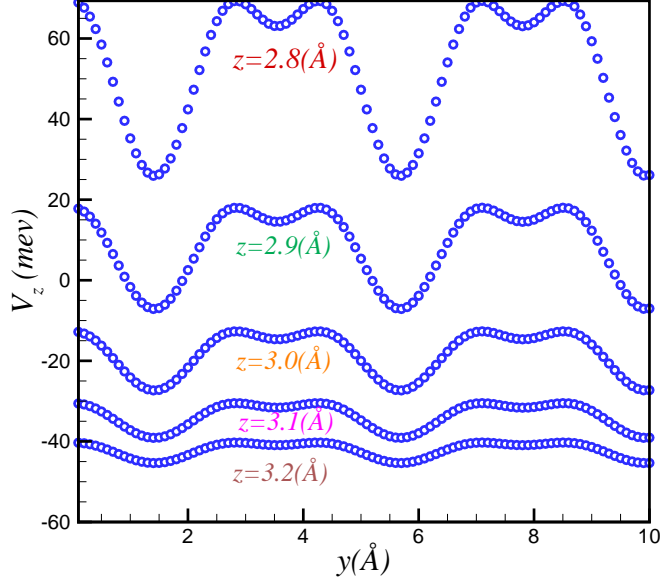


Figure 3: (Color online) Periodic potential energy between flat graphene sheet and a single carbon atom at  $x=0$  as a function of  $y$  for several height values.

the variation of potential energy in  $y$  direction at  $x = 0$  for five different heights. To show that the variation of  $\tilde{V}(x, y)$  in the  $z$  direction appears to be similar to the LJ potential, with different functionality, we averaged the above potential in the Wigner-Seitz primitive cells on both sublattices and plot the result in the bottom panel of Fig. 4. As can be seen from the figure the potential minimum between graphene sheet and the single carbon atom is deeper than the simple case of two interacting carbon atoms via the LJ interaction. Furthermore, the minimum distance ( $z_{min} \sim 3.4 \text{ \AA}$ ) is not  $z = 2^{1/6}\sigma \sim 3.8 \text{ \AA}$  as it is in the usual LJ (solid blue curve in Fig. 4). The minimum point of  $V_z$  gives the equilibrium distance of a carbon atom over graphene flat sheet.

Note that the particle will equilibrate with the graphene sheet and obtains a mean kinetic energy of the order of  $K_B T$  in its 2D lateral motion. If  $K_B T \simeq 25.7 \text{ meV}$  is smaller than the potential barriers heights, the particle may be trapped in one of the potential wells. Since  $\tilde{V}(x, y)$  is a two-dimensional potential, the particle could take various paths from one well to neighboring wells. But for simplicity we may roughly take the difference between maximum and minimum values of  $\tilde{V}(x, y)$  appearing in Wigner-Seitz primitive cells as a measure of the barrier strength compared to the thermal energy  $K_B T$ . The top panel in Fig. 4 shows the difference between maximum and minimum  $\Delta V$  in units of  $K_B T$  for various values of the particle height.

### 3.2 Potential energy between $C_{60}$ molecule and graphene sheet

In the case of molecules such as  $C_{60}$  as considered here, the total two-dimensional potential is periodic as well, see Fig. 5. The interaction between this molecule and the graphene sheet has several functional forms depending on the orientation of the molecule over the sheet even at a fixed height of the

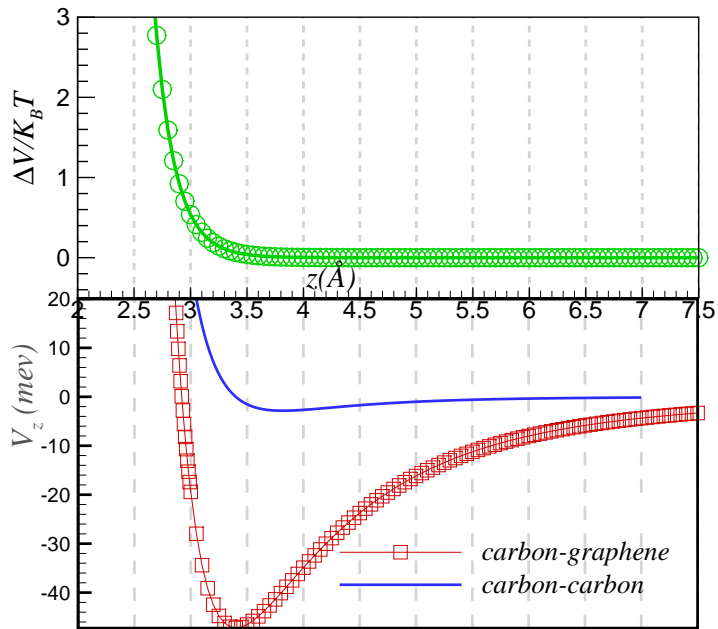


Figure 4: (Color online) Top: Difference between maximum and minimum of two-dimensional potential (averaged over Wigner-Seitz primitive cell of both A-lattice and B-lattice) created by a flat graphene sheet (see Fig. 2) as a function of normal distance  $z$  as experienced by a single carbon atom. Bottom: Total potential energy between a flat graphene sheet and a single carbon atom has been depicted. The solid blue curve is a simple LJ potential between two carbon atoms. In both panels, to eliminate the dependence on the  $x$  and  $y$  variables, we averaged over the first Brillouin zone of both A-lattice and B-lattice. The data have small ( $10^{-5}$ ) error bars which are not shown.

molecule's center of mass above the sheet. Two particular orientations of  $C_{60}$  are more interesting than the others. These two refer to the cases when a pentagon or a hexagon of  $C_{60}$ 's atoms faces the flat graphene surface. Figure 5 is related to a  $C_{60}$  molecule when one of the pentagons is near to the surface and the plane of the pentagon is parallel to the graphene sheet. Since the radius of the  $C_{60}$  molecule is  $R_{C_{60}}=3.54 \text{ \AA}$ , it can never get closer to the surface than this distance. Figure 6 shows the variation of potential energy along normal direction for five different height of the center of mass of  $C_{60}$  molecule. Furthermore the variation of  $E_T$  along  $z$  direction averaged over Wigner-Seitz primitive cells of A-lattice and B-lattice is shown in bottom panel of Fig. 7. This gives the minimum height value for the center of mass of  $C_{60}$  molecule as  $z_{min} \sim 6.5 \text{ \AA}$  which is obviously larger than the equilibrium distance obtained for a single carbon above the flat sheet. The binding energy of  $C_{60}$  molecule and monolayer graphene can be estimated around 800 meV which is the same to the experimental value for binding energy of  $C_{60}$  molecule and graphite bulk [9].

Similar to the the single carbon case we show the difference between maximum and minimum appearing in Wigner-Seitz primitive cells with respect to the thermal energy in top panel of Fig. 7. The several orientations have not much effects in the curves in Fig. 7. Furthermore, the height of saddle points in the potential profile in Fig. 5 with respect to the thermal energy is around 0.2, which indicates that thermal energy is the dominant factor. Therefore, we expect that there should not be

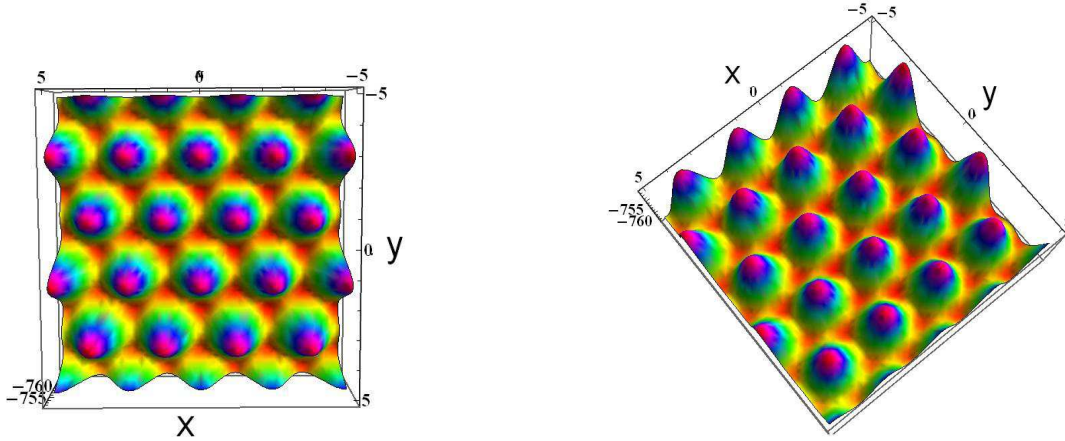


Figure 5: (Color online) Periodic two dimensional potential created by the graphene sheet. In this case  $x$  and  $y$  are the center of mass coordinates of  $C_{60}$  measured from an origin on the sheet at the height  $z = 6.5\text{\AA}$ . This is obtained by summing the potential experienced by all individual atoms comprising the  $C_{60}$  molecule. The panel in the left shows the top view of the potential, and the right panel shows the side view. The middle panel shows the potential energy between  $C_{60}$  molecule and flat graphene sheet at  $x=0$  as a function of  $y$  for several height values.

any trapping in the motion of  $C_{60}$  over graphene even at low temperatures and various orientations. In the next section we show that the motion coincides with a diffusive Brownian motion.

This foregoing observation about the size of  $C_{60}$  molecule and the ratio between thermal energy and the depth of the potential wells may be extended to other macromolecules and nanostructures such as bucky-balls and carbon nanotubes. Almost all of these carbon allotropes have longitudinal and lateral dimensions larger than those of  $C_{60}$ . In a future work we will investigate dynamics of other carbon allotropes over this mono layer sheet at finite temperatures.

## 4 Translational diffusion

In Fig. 8, the mean square displacement  $\langle R^2 \rangle$  of an ensemble of 30  $C_{60}$  molecules moving near a graphene sheet at room temperature is plotted as a function of time for the projected two dimensional motion onto the  $x$ - $y$  plane, where  $R^2 = x^2 + y^2$ . The inset of the figure shows  $x - y$  trajectory for a single  $C_{60}$  molecule. The total simulation time is 2.5 ns. Diffusion coefficient for the  $C_{60}$  molecule is obtained from this graph as  $D = 7.0 \times 10^{-10} \text{m}^2 \text{s}^{-1}$ . Using Einstein's relation, we estimate an effective friction coefficient of  $\xi = \frac{K_B T}{D} = 1.4 \times 10^9 \text{m}^{-2} \text{s} \times K_B T$  for  $C_{60}$  moving near a graphene sheet. At very short times the observed motion is not diffusive because we put all  $C_{60}$  at the center of the membrane with initial random velocities extracted from a Maxwell-Boltzman distribution, and the graphene is not in thermal equilibrium with those molecules. Therefore at very short time of about 5 ps, the  $C_{60}$  molecules attempt to find the minimum energy trajectories, yet their total displacement is not significant.

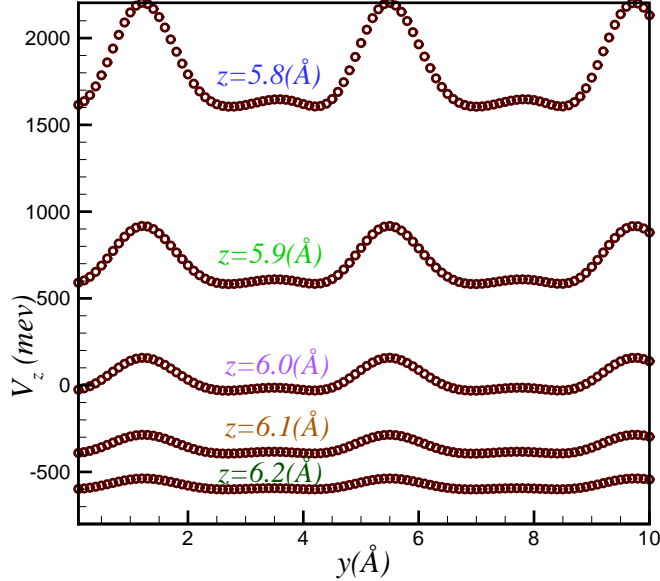


Figure 6: (Color online) Periodic potential energy between  $C_{60}$  molecule and flat graphene sheet at  $x=0$  as a function of  $y$  for several height values.

## 5 Effective potential for vibrational motion in $z$ -direction

In our MD simulations the  $C_{60}$  molecule does not unbind from the graphene sheet. We may introduce an effective potential for the  $C_{60}$  motion in the  $z$ -direction by calculating the distribution function,  $p(z)$ , of the height of a  $C_{60}$  above the sheet. By virtue of the Boltzmann factor, we may define the effective potential as  $\frac{U}{K_B T} = -\log[p(z)]$  which embeds in itself both entropic and energetic factors related to the equilibrated motion of  $C_{60}$  near the graphene sheet. Results are represented in Fig. 9. It turns that the effective potential has a harmonic-type shape and  $\frac{U}{K_B T} \cong \frac{1}{2}k(z - z_m)^2$  with the effective parameters  $k$  and  $z_0$  obtained from a best fit as  $k = 1.255K_B T$  ( $\text{N}/\text{\AA}$ ) and  $z_m = 5.908 \text{ \AA}$ . One thus expects that the  $C_{60}$  molecules effectively exhibit bounded vibrational motion in the normal direction to the graphene sheet. In lateral directions, as we discussed in the previous sections, the motion is diffusive. Here the mean value for  $\langle z \rangle = 5.975 \text{ \AA}$  shows the equilibrium distance of center of mass of  $C_{60}$  molecule which already has been thermalized with the graphene sheet. This value of height depends on the temperature of the system. Note that this equilibrium distance is calculated for the rough graphene unlike the value reported in section 3. The distance from graphene sheet is thus found to be bigger than the distance of  $C_{60}$  from the first layer of gold bulk [8], i.e.  $5.4 \text{ \AA}$ . This is because the graphene sheet is a single atomic layer instead of a bulk material.

## 6 Rotational diffusion

Rotation matrix transforms the coordinates of a vector in body-fixed frame to the coordinates in the lab-fixed frame. We define the body-fixed frame as two perpendicular vectors, which are chosen as two



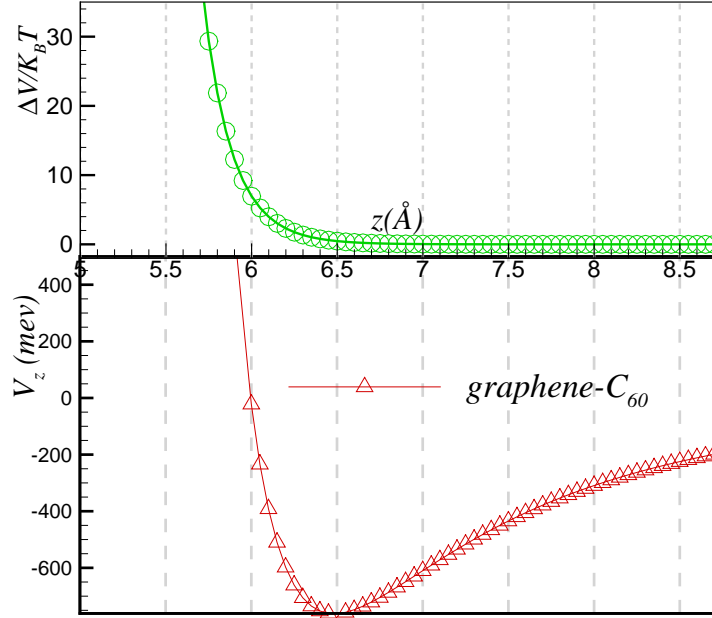


Figure 7: (Color online) Top: Difference between maximum and minimum of two-dimensional potential created by a flat graphene sheet (see Fig. 5) as a function of normal distance  $z$  as experienced by  $C_{60}$  molecule. Bottom: Total potential energy between a flat graphene sheet and a  $C_{60}$  molecule. In both panels, to eliminate the dependency of the  $x$  and  $y$  variables, we averaged over Wigner-Seitz primitive cells of both A-lattice and B-lattice with the data have infinitesimal ( $10^{-5}$ ) error bars which were not shown.

lines connecting two pairs of opposite points on the  $C_{60}$  cage and the cross vector of those two vectors. In order to be sure about the orthonormality of those vectors the Gram-Schmidt orthonormalization processes was applied in each time step of simulation.

The quaternion representation of rotation matrix is a useful method for numerical simulations since they are more numerically stable. [19]. The angular velocities of  $C_{60}$  in the body-fixed frame can be written in the term of quaternions and their time derivatives. Applying the inverse of the rotation matrix on the angular velocity of  $C_{60}$  in the body-fixed frame, yields the angular velocities of  $C_{60}$  in lab-fixed frame,  $\vec{\omega}$ .

To show that motion of  $C_{60}$  on the graphene is not a rolling motion, we have calculated the cross-correlation of the unit vector of angular velocity,  $\hat{\omega}$ , and the unit vector of velocity,  $\hat{v}$ , i.e.,  $\langle \hat{\omega} \cdot \hat{v} \rangle = 3.0 \times 10^{-2} \pm 0.01$  and  $\langle |\hat{\omega} \cdot \hat{v}| \rangle = 0.47 \pm 0.01$ . Note that the first average is almost zero but it can not confirm that these two vectors are uncorrelated because this average becomes zero for two perpendicular vectors as well. On the other hand, the non-zero second average shows that they are not perpendicular. Therefore, these two averages together make sure that these two vectors are uncorrelated. The independence of the direction of velocity from the angular velocity ensures that the motion of  $C_{60}$  over graphene sheet is not a rolling motion.

Defining a fixed vector in  $C_{60}$ ,  $\mu$ , helps us to investigate the diffusive nature of  $C_{60}$  motion. It can be understood from the time auto correlation of  $\mu$  where the correlation time is 37.5 ps (see Fig.

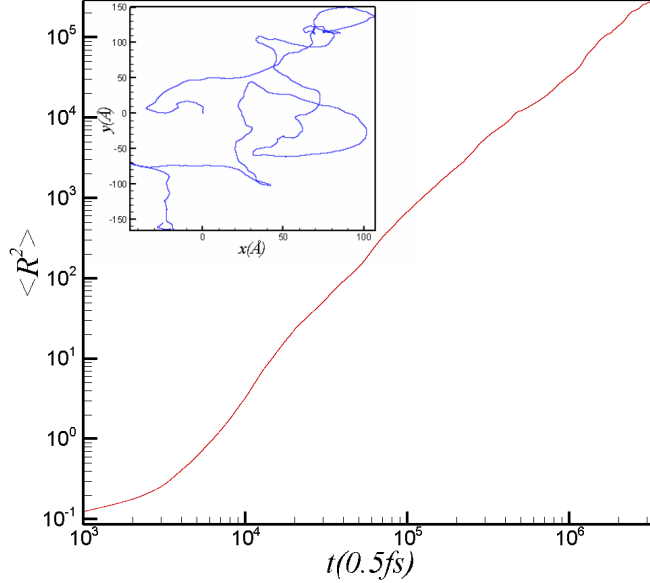


Figure 8: (Color online) Mean square displacement,  $\langle R^2 \rangle$ , versus time for the lateral motion of an ensemble of 30  $C_{60}$  molecules moving near a graphene sheet at room temperature. Inset show a typical  $x - y$  trajectory of a single  $C_{60}$  on the graphene sheet.

10). It is obvious that the correlation length of  $\mu$  is about 75000 steps which means that after this time the orientation of  $C_{60}$  becomes completely different. Angular velocity in different directions has different behaviors. Figure 11 shows the increment of  $\omega_z$  and  $\omega_{xy}$ . Obviously the fluctuations of  $\omega_z$  is bigger than  $\omega_{xy}$ . This is due to the structure of  $C_{60}$  which is not a continuous ball. It is a discrete spherical object. As we mentioned in the previous section the pairwise interaction of  $C_{60}$  with the graphene atoms depends on the several orientations of  $C_{60}$ . For example when a hexagon of  $C_{60}$  is parallel to another hexagonal in the graphene plane,  $C_{60}$  would be more stable than the other possible orientations. These restrictions do not affect the rotation around the  $z$  axis, so the rotation around the  $z$  axis is easier than around  $x - y$  direction.

## 7 Conclusion

We studied the motion of  $C_{60}$  molecule over a graphene sheet. Both flat approximation for monolayer graphene sheet and monolayer graphene at a finite temperature have been studied using atomistic simulations. The depth of the potential wells generated by a graphene sheet in its proximity decreases as the height of an external object increases above the sheet. The binding energy of  $C_{60}$  over a graphene sheet was found as 800 meV close to the experimental value for binding energy of  $C_{60}$  and graphite [9]. The motion of  $C_{60}$  in the perpendicular direction was found to be a vibrational motion similar to a simple harmonic oscillator. While the motion in lateral directions is found to be a diffusive non-rolling motion.

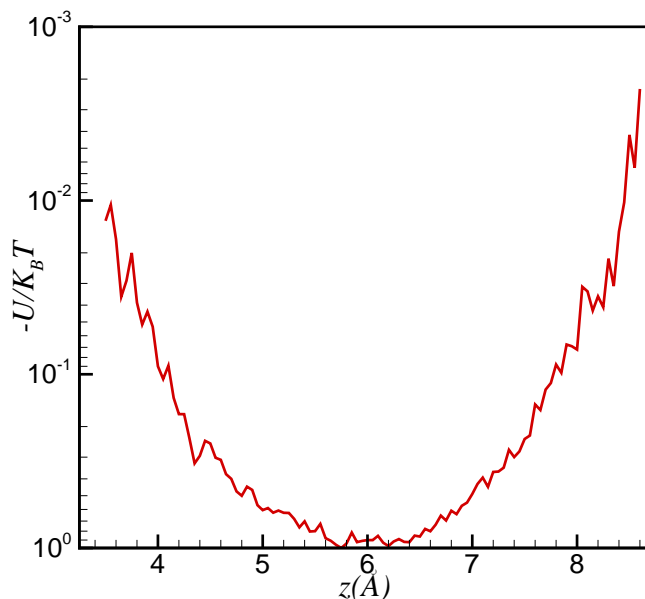


Figure 9: (Color online) Effective potential of the interaction between  $C_{60}$  molecule and a graphene sheet.

## References

- [1] K. S. Novoselov, A. K. Geim, S. V. Morozov, D. Jiang, Y. Zhang, S. V. Dubonos, I. V. Grigorieva, and A. A. Firsov, *Science* **306**, 666 (2004) .
- [2] A. K. Geim, and K. S. Novoselov, *Nature Mater.* **6**, 183 (2007) ; A. K. Geim and A. H. MacDonald, *Phys. Today* **60**, 35 (2007).; A. H. Castro Neto, F. Guinea, N. M. Peres, K. S. Novoselov, and A. K. Geim, *Rev. Mod. Phys.* **81**, 109 (2009) .
- [3] J. C. Meyer, C. O. Girit, M. F. Crommie and A. Zettl, *Letter Nature* **454**, 319-322 (2008).
- [4] E. Reister-Gottfried, SM. Leitenberger, and U. Seifert , *Phys. Rev. E* 75,011908 (2007).
- [5] E. Reister, and U. Seifert, *Europhys. Lett.* **71**, 859 (2005).
- [6] A. Naji, and F. L. H. Brown, *J. Chem. Phys.* **126**, 235103 (2007).; A. Naji, P. J. Atzberger, F. L. H. Brown, *Phys. Rev. Lett.* **102**, 138102 (2009).
- [7] A. Hashimoto, K. Lwao, S. Tanaka, and A. Yamamoto, *Diamond and Related Materials* **17**, 1622 (2008).
- [8] G. Teobaldi and, F. Zerbetto, *small*, **3**, 1694 - 1698 (2007).
- [9] H. Ulbricht, G. Moos, and T. Hertel, *Phys Rev Lett.* **7**, 90(9):095501 (2003).
- [10] Ch. Girard, Ph. Lambin, A. Dereux, and A. A. Lucas, *Phys. Rev. B*, **49**, 11425 (1994).

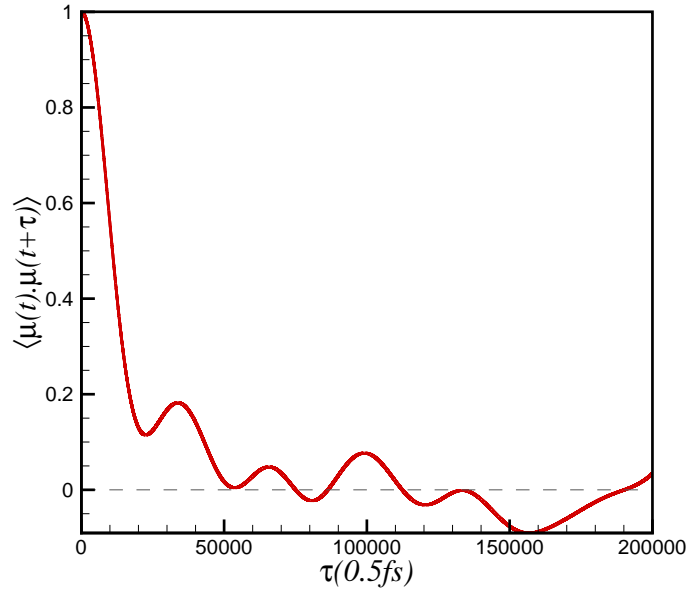


Figure 10: Rotational correlation: the correlation length of  $\mu$  is about 75000 steps (37.5 ps).

- [11] M Caragiu, and S Finberg , *J. Phys.: Condens. Matter* **17**, R995 (2005) and references therein.
- [12] K. S. Kim, J. C. Neu, and G. F. Oster, *Euro. Phys. Lett*, **48**, (1), 99-105 (1997).; *Bio. Phys. J*, **75**, 2274-2291 (1998).
- [13] O. Farago, *J. Chem. Phys*, **119**, 596-605 (2003).
- [14] A. M. L. Palacio, J. M. Sancho, M Igor Sokolov, and K Lindenberg, , *Phys. Rev .E* **70**, 051104 (2004)
- [15] H. Raffi-Tabar, *Physics Reports* **390**, 235 (2004).
- [16] M. Neek-Amal, R. Asgari, and M. R. Rahimi Tabar, *Nanotech.* **20**, 135602 (2009).
- [17] D. W. Brenner, *Phys. Rev. B* **42**, 9458 (1990) .
- [18] N. Abedpour, M. Neek-Amal, R. Asgari, F. Shahbazi, N. Nafari, and M. R. Tabar, *Phys. Rev. B* **76**, 195407 (2007)
- [19] D. C. Rapaport, *The art of molecular dynamics simulation*, (Cambridge University Press, 2004)

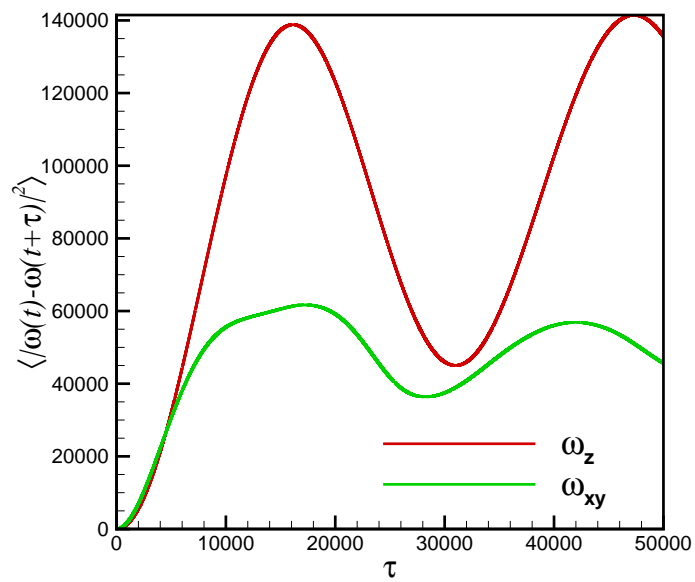


Figure 11: (Color online) Increment of  $\omega_z$  and  $\omega_{xy}$  versus time step.